NOAA Technical Report NESDIS 98

NOAA-L and NOAA-M AMSU-A Antenna Pattern Corrections

Washington, D.C.
August 2000

U.S. DEPARTMENT OF COMMERCE
National Oceanic and Atmospheric Administration
National Environmental Satellite, Data, and Information Service

NOAA TECHNICAL REPORTS

National Environmental Satellite, Data, and Information Service

The National Environmental Satellite, Data, and Information Service (NESDIS) manages the Nation's civil Earth-observing satellite systems, as well as global national data bases for meteorology, oceanography, geophysics, and solar-terrestrial sciences. From these sources, it develops and disseminates environmental data and information products critical to the protection of life and property, national defense, the national economy, energy development and distribution, global food supplies, and the development of natural resources.

Publication in the NOAA Technical Report series does not preclude later publication in scientific journals in expanded or modified form. The NESDIS series of NOAA Technical Reports is a continuation of the former NESS and EDIS series of NOAA Technical Reports and the NESC and EDS series of Environmental Science Services Administration (ESSA) Technical Reports.

A limited number of copies are available by contacting Nancy Everson, NOAA/NESDIS, E/RA, 5200 Auth Road, Camp Springs, Maryland 20746. Copies can also be ordered from the National Technical Information Service (NTIS), U.S. Department of Commerce, Sills Bldg., 5285 Port Royal Road, Springfield, VA. 22161, (703) 487-4650 (prices on request for paper copies or microfiche, please refer to PB number when ordering). A partial listing of more recent reports appear below:

NESDIS 55 Report of the Workshop on Radiometric Calibration of Satellite Sensors of Reflected Solar Radiation, March 27-28, 1990, Camp Springs, MD. P. Abel (Editor), July 1990.

NESDIS 56 A Noise Level Analysis of Special 10-Spin-Per-Channel VAS Data. Donald W. Hillger, James F. W. Purdom and Debra A. Lubich, February 1991.

NESDIS 57 Water vapor Imagery Interpretation and Applications to Weather Analysis and Forecasting. Roger B. Weldon and Susan J. Holmes, April 1991.

NESDIS 58 Evaluating the Design of Satellite Scanning Radiometers for Earth Radiation Budget Measurements with System, Simulations. Part 1: Instantaneous Estimates. Larry Stowe, Philip Ardanuy, Richard Hucek, Peter Abel and Herbert Jacobowitz, October 1991.

NESDIS 59 Interactive Digital Image Display and Analysis System (IDIDAS) User's Guide. Peter J. Celone and William Y. Tseng, October 1991.

NESDIS 60 International Dobson Data Workshop Summary Report. Robert D. Hudson (University of Maryland) and Walter G. Planet, February 1992.

NESDIS 61 Tropical Cyclogenesis in the Western North Pacific. Raymond M. Zehr, July 1992.

NESDIS 62 NOAA Workshop on Climate Scale Operational Precipitation and Water Vapor Products. Ralph Ferraro (Editor), October 1992.

NESDIS 63 A Systematic Satellite Approach for Estimating Central Pressures of Mid-Latitude Oceanic Storms. Frank J. Smigielski and H. Michael Mogil, December 1992.

NESDIS 64 Adjustment of TIROS Operational Vertical Sounder Data to a Vertical View. David Q.Wark, March 1993.

NESDIS 65 A Noise Level Analysis of Special Multiple-Spin VAS Data During Storm-fest. Donald W. Hillger, James F.W. Purdom and Debra A. Molenar, April 1993.

NESDIS 66 Catalogue of Heavy Rainfall Cases of Six Inches or more over the Continental U.S. during 1992. Charles Kadin, April 1993.

NESDIS 67 The Relationship between Water Vapor Plumes and Extreme Rainfall Events during the Summer Season. Wassila Thiao, Roderick A. Scofield and Jacob Robinson, May 1993.

NESDIS 68 AMSU-A Engineering Model Calibration. Tsan Mo, Michael P. Weinreb, Norman C. Grody and David Q. Wark, June 1993.

NOAA Technical Report NESDIS 98

NOAA-L and NOAA-M AMSU-A Antenna Pattern Corrections

Tsan Mo
Climate Research and Applications Division
Office of Research and Applications

Washington, D.C.
August 2000

U.S. DEPARTMENT OF COMMERCE
Norman Y. Mineta, Secretary

National Oceanic and Atmospheric Administration
D. James Baker, Under Secretary

National Environmental Satellite, Data, and Information Service
Gregory W. Withee, Assistant Administrator

TABLE OF CONTENTS

ABSTRACT 1

1. INTRODUCTION 2

2. ALGORITHM DEVELOPMENT 4

3. Description of Antenna Pattern Data 10

4. Results 12
   - 4.1 Beamwidth 12
   - 4.2 Main Beam Efficiencies 14
   - 4.3 Antenna Efficiencies over Earth, Cold Space, and Satellite Platform 14
   - 4.4 Antenna Pattern Corrections 16

5. Conclusion 19

ACKNOWLEDGMENT 20

REFERENCES 21

APPENDIX A 22

TABLE CAPTIONS

Table 1. NOAA-L AMSU-A1 PFM and AMSU-A2 FM1 channel characteristics. 3

Table 2. NOAA-L AMSU-A antenna efficiencies over the Earth, spacecraft, and space. 15

Table 3. NOAA-L AMSU-A: The η factor in Equation (12). 16

Table 4. NOAA-L: Cold space bias correction, $\Delta T_C(K)$, to the cosmic background temperature ($T_C = 2.73 + \Delta T_C$). 19

Table A-1. NOAA-M AMSU-A1 FM2 and AMSU-A2 FM2 channel characteristics. 23

Table A-2. NOAA-M AMSU-A antenna efficiencies over Earth, spacecraft, and space. 24

Table A-3. NOAA-M AMSU-A: The η factor in Eq. (12). 25

Table A-4. NOAA-M: Cold space bias correction, $\Delta T_C(K)$, to the cosmic background temperature ($T_C = 2.73 + \Delta T_C$). 25

FIGURE CAPTIONS

Figure 1. Geometric sketch of the satellite and Earth relationship.. 5

Figure 2. Sample of antenna pattern data from AMSU-A1 PFM Channel 3 (50.3 GHz). 13

Figure 3. Sample of calculated NOAA-L antenna pattern corrections $\Delta T = T_B - T_A$ for one scan line. 18

Figure A-1. Sample of antenna pattern data from AMSU-A1 FM2 Channel 3 (50.3 GHz). . . . 26

Figure A-2. Sample of calculated NOAA-M antenna pattern corrections $\Delta T = T_B - T_A$ for one scan line. 27

NOAA-L and NOAA-M AMSU-A Antenna Pattern Corrections

Tsan Mo
Climate Research and Applications Division
Office of Research and Applications
NESDIS/NOAA
5200 Auth Road, Camp Springs, MD 20746

ABSTRACT

A procedure for making antenna pattern corrections to antenna temperatures of the Advanced Microwave Sounding Unit-A (AMSU-A) is presented. Antenna efficiencies, fractions of total power, over three different solid-angle regions subtended at the satellite by the Earth, cold space, and the satellite platform were calculated at thirty Earth views and four possible cold space calibration positions. These calculated results simplify the process for correcting antenna temperature measurements to retrieve the true brightness temperatures from AMSU-A data.

1. INTRODUCTION

In May 1998, NOAA launched the first of a new generation of total-power microwave radiometers, the Advanced Microwave Sounding Unit-A (AMSU-A), on its NOAA-K, L, M, N and N' series of Polar-orbiting Operational Environmental Satellites (POES). Each AMSU-A instrument consists of two separate units, AMSU-A2 with two channels at 23.8 and 31.4 GHz, and AMSU-A1 with twelve channels in the range of 50.3 to 57.3 GHz and another one at 89.0 GHz. Totally, AMSU-A furnishes fifteen channels. Description of the AMSU-A instrument and its radiometric performance has been reported elsewhere [1]. In tandem with each AMSU-A, there is also an AMSU-B, which has five channels with two channels at 89 and 150 GHz, and three channels around the 183 GHz water vapor lines. AMSU-B, which is provided by the U. K. Meteorological Office, is for humidity sounding and has been described elsewhere [2]. Only a brief description of the AMSU-A instruments is given here.

AMSU-A1 uses two antenna systems to provide the twelve oxygen band channels (3-14) for retrieving the atmospheric temperature profile from the Earth's surface to about 50 kilometer (km), or from 1000 to 1 millibar (mb). The remaining three channels (1 and 2 from A2; and 15 from A1) aid the retrieval of temperature soundings by the correction of surface emissivity, atmospheric liquid water, and total precipitable water. These window channels also provide information on precipitation, sea ice, and snow coverage.

Table 1 lists some of the main NOAA-L AMSU-A channel characteristics, which include the channel frequency, number of bands, band width, and radiometric temperature sensitivity (or NEΔT) for each channel. Similar results for NOAA-M AMSU-A are given in Appendix A. Each antenna system consists of an offset parabolic reflector housed in a cylindrical shroud. The reflectors rotate one complete revolution every 8 seconds during which 30 Earth scenes (also referred to as beam positions, within $\pm 48°20'$ from nadir and each separated by 3°20') will be sampled in a stepped-scan fashion. Data for onboard calibration are obtained from views of cold space and a blackbody target once every 8 seconds at the end of each scan line. Beam positions 1 and 30 are the extreme scan positions of the Earth views, while beam positions 15 and 16 are at 1°40' and -1°40' from the nadir direction, respectively.

Measurement of the antenna pattern is an important part the AMSU-A calibration process. AMSU-A specification requires that the antenna beam width at half-maximum points (3-dB width) should be

Table 1. NOAA-L AMSU-A1 PFM and AMSU-A2 FM1 channel characteristics.

Channel Number	Channel Frequency (MHz)		No. of Bands	Measured 3-dB RF Bandwidth (MHz)	NEΔT (K)		Beam # Efficiency	Polarization (NADIR)	FOV** (deg.)	Remarks
	Specification	Measured *			Spec.	Measred				
1	23800	23800.11	1	250.90	0.30	0.166	96%	V	3.42	A2 FM1
2	31400	31400.58	1	161.40	0.30	0.203	97%	V	3.52	"
3	50300	50299.7	1	161.16	0.40	0.227	96%	V	3.60	A1-2 PFM
4	52800	52800.74	1	380.50	0.25	0.138	96%	V	3.55	"
5	53596 ± 115	53595.47 ± 115	2	168.26 I 168.26	0.25	0.154	96%	H	3.54	"
6	54400	54399.78	1	380.60	0.25	0.131	96%	H	3.47	A1-1 PFM
7	54940	54940.77	1	380.62	0.25	0.133	96%	V	3.47	"
8	55500	55499.54	1	310.16	0.25	0.142	96%	H	3.59	A1-2 PFM
9	fo = 57290.344	fo = 57290.334	1	310.60	0.25	0.157	96%	H	3.40	A1-1 PFM
10	fo ± 217	fo ± 217	2	76.69 I 76.69	0.40	0.210		H		"
11	fo ± 322.2 ± 48	fo ± 322.2 ± 48	4	34.49 / 34.64 I 34.64 / 34.49	0.40	0.235		H		"
12	fo ± 322.2 ± 22	fo ± 322.2 ± 22	4	15.01 / 15.31 I 15.31 / 15.01	0.60	0.344		H		"
13	fo ± 322.2 ± 10	fo ± 322.2 ± 10	4	7.90 / 7.97 I 7.97 / 7.90	0.80	0.477		H		"
14	fo ± 322.2 ± 4.5	fo ± 322.2 ± 4.5	4	2.89 / 2.93 I 2.93 / 2.89	1.20	0.768		H		"
15	89000	88999.80	1	1994.04	0.50	0.152	98%	V	3.29	"

Measured at temperature 18°C. ** Specification= 3.3° ±10% for all channels. # Measured

3.3°±10% and that the main beam efficiency, which is defined as the ratio of the power (including both co- and cross-polarizations) received by an antenna within its main beam to the total power received from all solid angles, must be ≥95%. Here, the main beam is defined as 2.5 times the 3-dB beamwidth. The remaining portion (≈5%) of the total power received by the antenna via its side lobes originates from a wide angular range that includes the satellite platform and cold space (sky), where the cosmic background brightness temperature, 2.73K, is considerably less than the Earth's temperatures. In a previous study [3], a procedure for making the antenna pattern side-lobe corrections to the antenna temperatures at 30 Earth scenes from the NOAA-K AMSU-A was developed. Following the same process, we studied the NOAA-L and -M AMSU-A antenna pattern corrections. The main beam efficiency and 3-dB beamwidth for each channel were also calculated for comparison with the AMSU-A specifications.

2. ALGORITHM DEVELOPMENT

The approach for formulating the procedures in making the antenna pattern corrections for the AMSU-A instrument has been given elsewhere [3]. Only a brief description of the appropriate formulas for calculating the antenna pattern corrections is presented in this section

A geometric sketch of the scanning AMSU-A antenna on a satellite is shown in Figure 1, where the satellite, S, is at a height $h = \overline{HS}$ ($h \approx 833$ and 870 km for morning and afternoon POES, respectively) above the Earth's surface. A Cartesian coordinate system $x'y'z'$ is placed at the Earth's center O. We assume that the y'-z' plane contains the POES's orbit. Without loss of generality, the AMSU-A antenna boresight is assumed to scan crosstrack in the x'-z' plane to acquire data at 30 Earth views, cold space and the blackbody target, respectively. For convenience, a second coordinate system xyz, which is parallel to the first set, is attached to the satellite S. Another coordinate system uvw, which is useful in performing integrations involving antenna pattern functions, is obtained by rotating the x-z plane around the y-axis by an angle β (defined below). After this rotation, the w-axis aligns with the negative boresight direction.

Assume that the AMSU-A antenna system looks at the boresight direction B (in the x-z plane), which makes a scan angle β ($=\angle OSB$) with the nadir (or -z axis). Let P denote a general ray pointing at an arbitrary direction defined by $\Omega = (\theta, \phi)$, where θ is the angle $\angle OSP$ measured from the nadir and

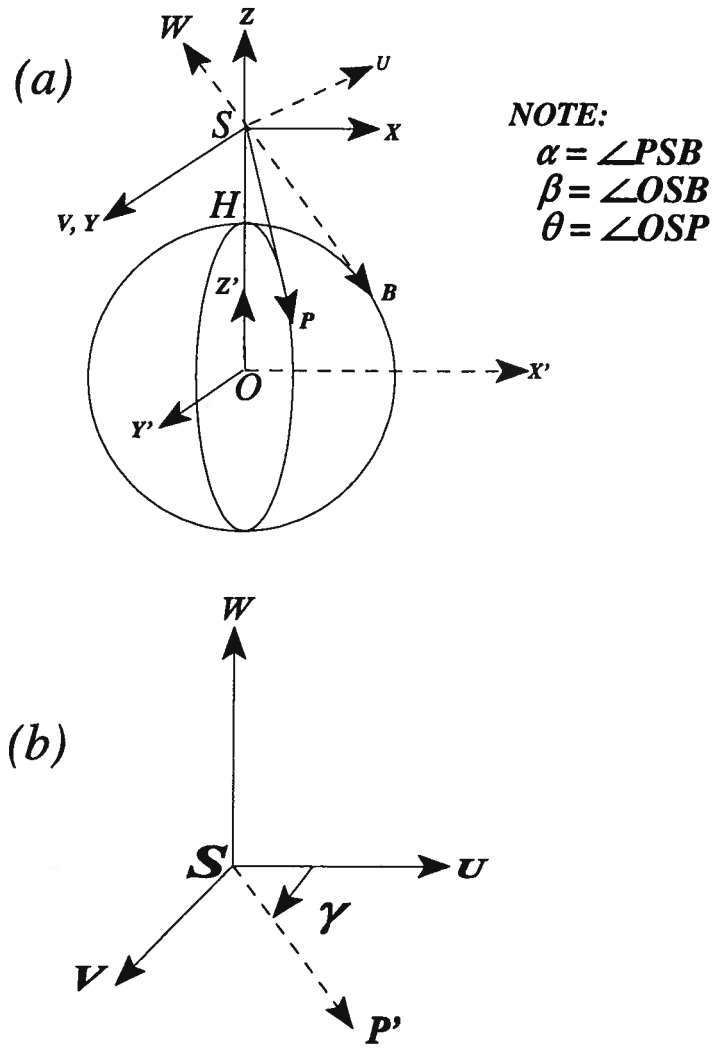

Figure 1. (a) Geometric sketch of the satellite and Earth relationship. (b) Define the angle γ in the uvw coordinate system. The vector SP' is the projection of SP on the u-v plane.

where

$$g(\theta) = \int_0^{2\pi} G(\alpha,\gamma)\,d\phi \qquad \textbf{(10)}$$

The antenna temperature $T_A(\beta)$ in Equation (9) consists of three components which are represented by the three integrals on the right-hand side, where the $T_E(\theta)$, T_C, and T_{sat} denote the brightness temperatures of the Earth, cold space and satellite platform, respectively. The integration limit θ_{max} in Equation (9) is the half-cone angle subtended by the Earth and 20-km atmosphere at the satellite which is at a height of h ≈ 870 km above the Earth's surface for NOAA-L. Following previous reports [7], the atmosphere below 20 km is considered as an extended shell of the Earth for computing the antenna pattern side-lobe corrections. It can be shown from Figure 1 that θ_{max} is defined by

$$\theta_{max} = \sin^{-1}\left(\frac{R+20}{R+h}\right) \qquad \textbf{(11)}$$

where R is the Earth's radius and h the height of the satellite. This gives $\theta_{max} = 61.96°$ with R=6371.2 km. The factor (R+20) on the numerator indicates that the half-cone angle is extended beyond the Earth's surface to include the atmosphere below 20 km.

Equations (1) and (9) are given in terms of brightness temperatures, but both are still valid if all temperatures are replaced by their corresponding radiance. The conversion between radiance and temperature are via the Planck function. Since the Rayleigh-Jeans approximation breaks down at the cold space temperature (~2.73K), we did all calculations in radiance, which were then converted into temperatures as the final products.

Equation (9) gives a good representation for simulating the antenna temperature if the brightness temperatures $T_E(\theta)$, T_C, and T_{sat} are known. The last two quantities are approximately constant over the range of individual integrations, but $T_E(\theta)$ may vary considerably over its integration limits. However, the AMSU-A antenna patterns are all sharply peaked and decrease rapidly as the scan angle moves away from the boresight direction. Thus, $T_E(\theta)$ can be approximated by a constant $\overline{T}_E$, which represents a mean atmospheric brightness temperature for each channel in the neighborhood of boresight direction β when it is on the Earth views. On the other hand, if the boresight direction is on a space view when the T_A is calculated, the Earth contribution comes mainly from the limb, which,

in our case, is the atmosphere at 20 km above the Earth's surface, where brightness temperature is approximately 210K. Therefore, $T_E = 210K$ should be used when T_A is calculated at the four space views.

The above discussion assumes all radiation sources being far away from the antenna system (i.e.,in the "far field"). However, the satellite platform, which is in the "near-field" of the antenna, alters its far-field radiation pattern. Ideally, one should use the far-field patterns measured with a mock-up of the satellite platform attached to the antenna. However, such a measurement would be costly and may be impossible. Computer simulation is an alternative approach, which was performed at one of the cold space calibration positions by the instrument manufacturer. Its result showed that the near-field effect of the satellite platform reduces the contribution [8]-[11] from the last integration in Equation (9). To match this computer simulated result of near-field effect, a scale factor η is introduced into the last term in Equation (9). The η values for individual channels will given in Section 4.3. Then it is reasonable to approximate the integrations in Equation (9) as a combination of three parts each of which represents a weighted mean brightness temperature within its integration region,

$$T_A(\beta) = \frac{1}{N_\eta}\left[f_e(\beta)\,\overline{T}_E + f_c(\beta)\,\overline{T}_C + \eta f_{sat}(\beta)\,\overline{T}_{Sat}\right] \qquad \textbf{(12)}$$

where N_η is a renormalization factor, which is necessary because of the inclusion of the scale factor η, and it is defined as

$$N_\eta = f_e(\beta) + f_c(\beta) + \eta f_{sat}(\beta) \qquad \textbf{(13)}$$

The corresponding antenna efficiencies, $f_x(\beta)$, where x = e, c, or sat, in Equation (12), are defined by,

$$f_x(\beta) = \frac{1}{N}\int_{\theta_x} g(\theta)\sin\theta\, d\theta \qquad \textbf{(14)}$$

where the integration limit θ_x (with x = e, c, or sat) corresponds to the one for Earth, cold space, or satellite platform, respectively, as given in Equation (9). The antenna efficiencies $f_x(\beta)$ were computed at the 30 Earth views and 4 cold calibration positions for all channels, of which antenna

pattern data are available. Then, we can compute corrections for both the Earth views and cold space views. It should be noted that normalization requires $f_e(\beta) + f_c(\beta) + f_{sat}(\beta) = 1$ for a fixed β value.

In Equation (12), the $\overline{T}_C$ (=2.73K) is the cold space temperature. The $\overline{T}_{Sat}$ represents the total energy emanation associated with the satellite platform and it may consist of satellite-platform radiation as well as reflection of radiations from the Earth and cold space. It has been shown elsewhere [3] that the maximum contribution from the last term in Equation (12) is of the order of 0.01K, which is less than the NEΔT. In practice, this term can be ignored in comparison with the NEΔT uncertainties. The calculated result presented below is considered accurate, but it is subject to possible errors in the above assumptions. Data users, who want more accurate results, should perform their own calculations, using the $\overline{T}_E$ and $\overline{T}_{Sat}$ values, which may be more appropriate to the actual environmental conditions at the data collection time and location.

Main beam efficiency is another important characteristics of the antenna pattern function. It is defined as the ratio of the power received within the main beamwidth to the total power from all angles collected by the antenna system, including both co- and cross-polarized power. Here, the main beamwidth is defined as 2.5 times the measured 3-dB beamwidth of an antenna pattern. Practically, the main beam efficiency can be calculated from Equation (14) by replacing the integration limit with a half-cone angle equal to 1.25 times the 3-dB beamwidth. This is defined as

$$f_{main}(\beta) = \frac{1}{N}\int_0^{\theta_{main}} g(\theta)\sin\theta\, d\theta \qquad \textbf{(15)}$$

where θ_{main} equals 1.25 times the 3-dB beamwidth for individual channels, as given in Table 1.

3. Description of Antenna Pattern Data

The NOAA-L AMSU-A instrument consists of the A2 Flight Model 1 (FM1) and A1 Proto-Flight Model (PFM) whereas NOAA-M has AMSU-A1 FM2 and A2 FM2. Antenna pattern data for both models were measured by Aerojet, the instrument's manufacturer. Detailed description of the data measurement process was given elsewhere [12]. Only a brief description of the measurements is presented here.

The antenna pattern data were measured at each channel frequency, except channels 9 through 14 which share the same central frequency (57.29 GHz). Therefore, the antenna pattern data used in this study consist of ten channels with different central frequencies. The measurements were performed at the Intermediate Frequency (IF) outputs of the mixer/amplifiers. A spectrum analyzer was used to accommodate testing at the IF outputs of the instrument. To achieve the required 55 dB dynamic range for these measurements, the patterns were measured in two parts: (1) in the main beam region, a 20 dB of attenuation was inserted in the range transmitter and (2) in the sidelobe region, the attenuation was removed. The measurement process starts with the operator positioning the antenna at the peak of the beam with 20 dB of attenuation inserted before the transmit horn of the measurement system, at which point he begins the test on the antenna range controller that measures the power received at this point and sets this power level to the top of the scale on the spectrum analyzer. The controller then moves the antenna positioner and measures the antenna pattern for an angular span of 10 degrees centered on the peak of the beam with an increment size of 0.2°. The angular span of 10° was selected because it covers the 20-30 dB range of the central antenna pattern. The data were digitally recorded and read from the spectrum analyzer. At the second step of the measurement, the 20-dB attenuator is removed and the antenna patterns over the other angular spans are measured. The controller measures the power level received from the spectrum analyzer at each measurement and subtracts 20 dB from this reading and stores the results. At each of these ten channel frequencies, the measured data consist of elements as follows,

- Four planes: At each frequency, antenna pattern data were measured at 4 plane "cuts". Each cut corresponds to two azimuthal angles, i.e., $\gamma = 0$ and 180, 45 and 225, 90 and 270, and 135 and 315 degrees, respectively. These plane-cuts will be referred to as the 0°, 45° 90°, and 135° cuts, respectively
- Angular range and scan interval: The scanning angle (i.e. α) extends from 0° to ±180° from the antenna boresight with 0.2° steps
- Fine-step data: For accurate determination of the antenna beam widths, the central parts of the antenna pattern (0° to ±4.5°) were measured at steps of 0.05°. These fine-step data were measured at two plane cuts, crosstrack (γ=0°) and downtrack (γ=90°) cuts.
- Three beam positions: Data were taken at three Earth viewing beam positions, 1, 15, and 30.
- Two polarizations: Each set of these antenna patterns was measured with two different polarizations (co- and cross-polarizations).

Figure 2 shows a sample of the antenna pattern data, which were measured at the frequency of 50.3 GHz (Channel 3) at beam position 30 for all four cuts. The 0°-cut corresponds to the cross-track scan plane while the 90°-cut is in the down-track plane. At each cut, the central peak of the co-polarization power was normalized to 0 dB, with respect to which all other data points were scaled. The co-polarization data are shown in the column on left-hand side while the cross polarizations are displayed on right-hand side. Results in Figures 2 show that the cross-polarization spectra are approximately 20 dB smaller than the corresponding ones in co-polarization in the main lobe. However, the cross- and co-polarized power signals in the side lobes at large scan angles have about the same magnitudes.

4. Results

The formulas developed in Section 2 were used to generate the results described in this section. The antenna pattern data described above were also used to calculate the 3-dB beamwidth, and the main beam efficiencies. Calculations of antenna efficiencies over three different solid-angle regions subtended at the satellite by the Earth (plus the atmosphere below 20 km), cold space, and the satellite platform are performed at 30 Earth views and 4 cold space views. These calculated antenna efficiencies were then used to simulate the AMSU-A antenna temperatures.

4.1 Beamwidth

The 3-dB beamwidth is defined as the full angular width between two angles where the magnitude of antenna pattern drops to one half of its peak value at boresight. The fine-step antenna data were used in determination of individual channel 3-dB beamwidth. Linear interpolation of the fine-step data was used to determine the exact half-power locations. Table 1 lists these measured 3-dB beamwidth at beam position 15 for all channels, except channels 10-14, which share the same central frequency as channel 9. No measurement of antenna pattern was made for these channels. The channel central frequencies are also listed in Table 1.

AMSU-A specification requires 3.3°±10% for the 3-dB beamwidth. Table 1 shows that the beamwidths at all channels are within specification.

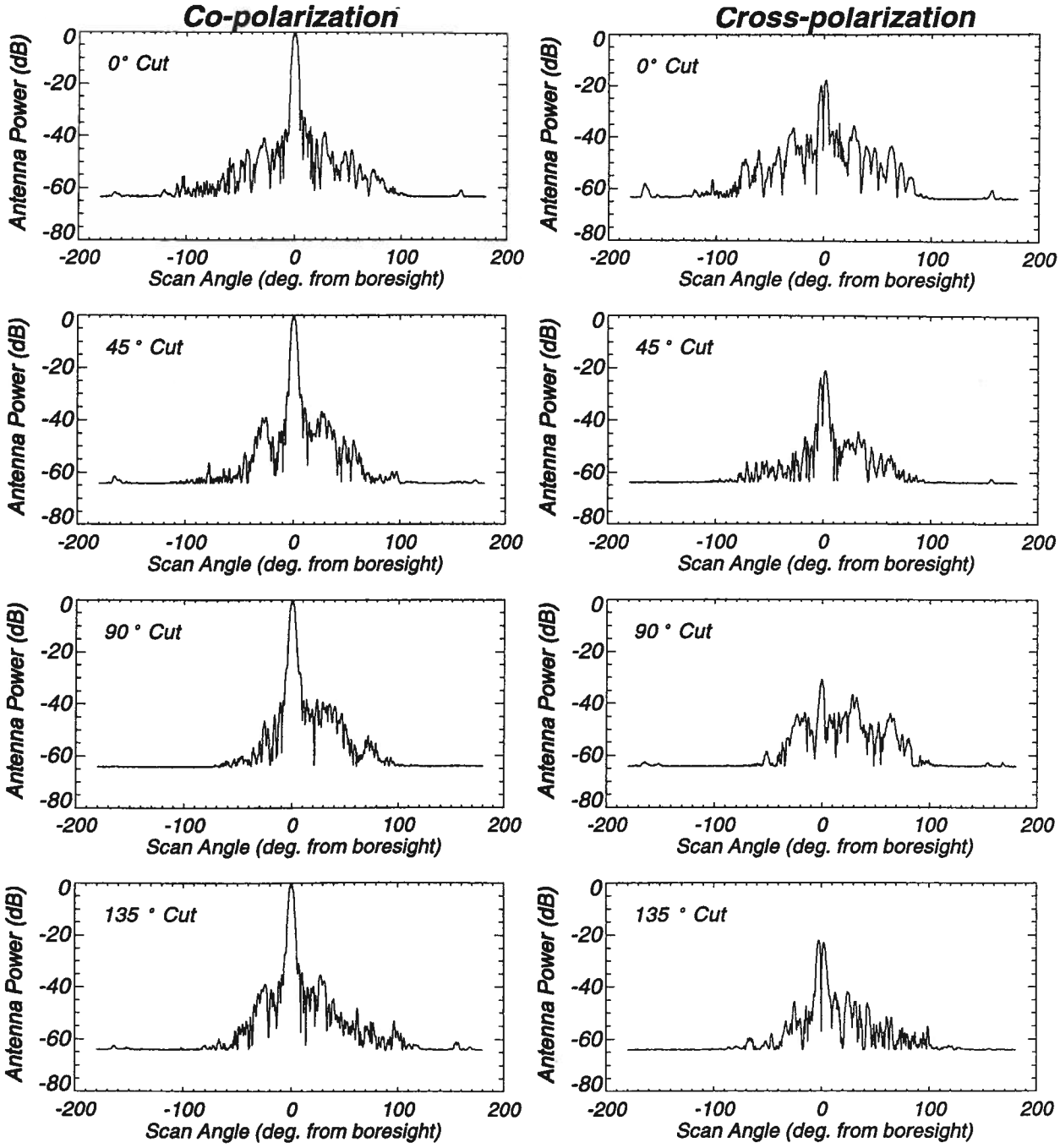

Figure 2. Sample of antenna pattern data from AMSU-A1 PFM Channel 3 (50.3 GHz) . The left-hand column shows the co-polarized data whereas the cross-polarized data are displayed in the right-hand column.

4.2 Main Beam Efficiencies

The main beam efficiency is defined in Equation (15) with θ_{main} equal to 1.25 times the 3-dB beamwidth at each channel. With the 3-dB beamwidth in Table 1, the main beam efficiencies for the channels were calculated.

AMSU-A specification requires that the main beam efficiencies should be ≥95% for all channels. The results in Table 1 meet the specification.

4.3 Antenna Efficiencies over Earth, Cold Space, and Satellite Platform

The antenna efficiencies integrated over the Earth (plus 20-km atmosphere), cold space, and satellite platform were calculated from Equation (14). Results of the three antenna efficiencies, $f_e(\beta)$, $f_c(\beta)$, and $f_{sat}(\beta)$ for NOAA-L AMSU-A are listed in Table 2 for 30 Earth viewing positions and 4 cold sky calibration positions. Similar results for NOAA-M AMSU-A are presented in Appendix A.

The f_{sat} values (Table 2) at the cold calibration positions are in the order of 1% without including the near-field effect of the satellite platform. During the calibration process, Aerojet performed a computer simulation of this near-field effect on the antenna efficiency and calculated one set of the f_{sat} values at the cold calibration position CC1 for individual channels [[8]-[11]. These calculated results for NOAA-L AMSU-A are listed in Table 3 in the second column which is labeled as f_{Asat}.

For comparison, the corresponding f_{sat} values at CC1 from Table 2 are listed in the third column in Table 3. One can see that the near field effect reduces the contribution from the satellite platform. To reduce the f_{sat} values to the same magnitude as those of the computer simulated results, we define the scale factor η, which appears in Equation (12) as

$$\eta = \frac{f_{Asat}}{f_{sat}} \qquad \textbf{(16)}$$

The η values for all channels are list in the last column in Table 3. These η values will be included in computing the antenna temperatures from Equation (12).

Table 2. NOAA-L AMSU-A antenna efficiencies over the Earth, space craft, and cold space. Note that cc represents the cold calibration position.

Beam Pos.	Scan Angle (deg.)	Ch.1			Ch.2			Ch.3			Ch.4			Ch.5		
		Fearth (%)	Fsat (%)	Fspace (%)	Fearth (%)	Fsat (%)	Fspace (%)	Fearth (%)	Fsat (%)	Fspace (%)	Fearth (%)	Fsat (%)	Fspace (%)	Fearth (%)	Fsat (%)	Fspace (%)
1	48.33	98.78	0.31	0.91	99.38	0.13	0.49	98.88	0.29	0.83	99.22	0.13	0.65	99.05	0.19	0.76
2	45.00	98.87	0.27	0.86	99.43	0.11	0.46	98.98	0.27	0.75	99.31	0.12	0.57	99.13	0.16	0.71
3	41.67	98.96	0.23	0.81	99.48	0.10	0.42	99.05	0.24	0.71	99.37	0.12	0.52	99.20	0.14	0.66
4	38.33	99.07	0.21	0.73	99.52	0.09	0.39	99.14	0.23	0.63	99.44	0.11	0.45	99.28	0.13	0.59
5	35.00	99.15	0.18	0.67	99.55	0.08	0.38	99.28	0.21	0.52	99.52	0.10	0.38	99.38	0.12	0.50
6	31.67	99.22	0.16	0.62	99.57	0.07	0.36	99.43	0.20	0.36	99.61	0.10	0.29	99.50	0.11	0.39
7	28.33	99.26	0.15	0.59	99.60	0.07	0.33	99.49	0.18	0.33	99.68	0.09	0.23	99.56	0.11	0.34
8	25.00	99.31	0.13	0.56	99.61	0.06	0.32	99.50	0.15	0.35	99.70	0.09	0.21	99.58	0.11	0.31
9	21.67	99.38	0.12	0.50	99.65	0.06	0.29	99.53	0.14	0.33	99.72	0.09	0.19	99.59	0.10	0.30
10	18.33	99.42	0.11	0.47	99.67	0.06	0.27	99.54	0.14	0.32	99.72	0.09	0.19	99.61	0.10	0.29
11	15.00	99.47	0.11	0.42	99.68	0.06	0.26	99.56	0.13	0.31	99.71	0.09	0.19	99.63	0.09	0.28
12	11.67	99.49	0.11	0.40	99.68	0.06	0.27	99.57	0.13	0.30	99.71	0.10	0.19	99.64	0.09	0.27
13	8.33	99.51	0.11	0.38	99.68	0.06	0.26	99.56	0.13	0.31	99.71	0.10	0.19	99.64	0.09	0.27
14	5.00	99.52	0.11	0.37	99.68	0.06	0.26	99.57	0.13	0.30	99.71	0.10	0.19	99.63	0.09	0.27
15	1.67	99.52	0.11	0.37	99.66	0.07	0.27	99.57	0.13	0.30	99.71	0.10	0.19	99.63	0.10	0.28
16	-1.67	99.53	0.11	0.36	99.66	0.07	0.28	99.58	0.14	0.28	99.69	0.11	0.21	99.63	0.10	0.28
17	-5.00	99.54	0.11	0.36	99.66	0.07	0.27	99.59	0.14	0.27	99.64	0.11	0.25	99.62	0.10	0.28
18	-8.33	99.54	0.11	0.35	99.65	0.07	0.28	99.59	0.14	0.27	99.62	0.11	0.28	99.61	0.10	0.29
19	-11.67	99.52	0.11	0.37	99.65	0.07	0.28	99.59	0.14	0.27	99.60	0.11	0.29	99.61	0.10	0.29
20	-15.00	99.50	0.11	0.38	99.63	0.08	0.29	99.59	0.15	0.27	99.59	0.12	0.29	99.60	0.11	0.29
21	-18.33	99.45	0.12	0.42	99.61	0.09	0.30	99.57	0.16	0.28	99.57	0.13	0.30	99.58	0.12	0.31
22	-21.67	99.41	0.13	0.46	99.59	0.09	0.31	99.52	0.17	0.30	99.54	0.14	0.32	99.56	0.13	0.32
23	-25.00	99.35	0.14	0.51	99.57	0.10	0.33	99.50	0.18	0.32	99.52	0.15	0.33	99.54	0.14	0.32
24	-28.33	99.26	0.15	0.59	99.53	0.11	0.36	99.47	0.19	0.34	99.50	0.16	0.35	99.52	0.15	0.33
25	-31.67	99.17	0.16	0.67	99.49	0.12	0.40	99.37	0.22	0.41	99.45	0.18	0.37	99.47	0.16	0.37
26	-35.00	99.09	0.17	0.74	99.43	0.13	0.44	99.19	0.23	0.58	99.35	0.21	0.44	99.34	0.18	0.48
27	-38.33	98.99	0.19	0.82	99.39	0.14	0.47	99.05	0.24	0.71	99.23	0.23	0.54	99.21	0.19	0.60
28	-41.67	98.91	0.21	0.88	99.34	0.16	0.51	98.92	0.26	0.82	99.15	0.25	0.60	99.10	0.20	0.70
29	-45.00	98.80	0.25	0.95	99.28	0.18	0.53	98.82	0.27	0.91	99.07	0.27	0.65	99.00	0.22	0.78
30	-48.33	98.68	0.29	1.03	99.23	0.21	0.57	98.71	0.31	0.98	99.00	0.30	0.71	98.90	0.24	0.86
CC4	-76.67	0.90	1.07	98.02	0.40	0.63	98.97	0.90	1.10	98.00	0.55	0.83	98.62	0.67	0.88	98.45
CC3	-80.00	0.80	1.19	98.00	0.34	0.70	98.96	0.82	1.21	97.97	0.49	0.91	98.60	0.60	1.01	98.39
CC2	-81.67	0.75	1.26	98.00	0.31	0.74	98.95	0.77	1.27	97.96	0.46	0.95	98.59	0.57	1.08	98.35
CC1	-83.33	0.69	1.34	97.97	0.29	0.78	98.93	0.73	1.33	97.95	0.43	1.00	98.57	0.53	1.16	98.30

Beam Pos.	Scan Angle (deg.)	Ch. 6			Ch. 7			Ch. 8			Ch. 9			Ch. 15		
		Fearth (%)	Fsat (%)	Fspace (%)	Fearth (%)	Fsat (%)	Fspace (%)	Fearth (%)	Fsat (%)	Fspace (%)	Fearth (%)	Fsat (%)	Fspace (%)	Fearth (%)	Fsat (%)	Fspace (%)
1	48.33	99.22	0.17	0.61	99.14	0.20	0.66	99.09	0.18	0.73	99.03	0.32	0.65	99.53	0.22	0.25
2	45.00	99.30	0.16	0.54	99.21	0.18	0.61	99.17	0.16	0.67	99.09	0.31	0.60	99.54	0.22	0.23
3	41.67	99.38	0.15	0.47	99.27	0.17	0.56	99.26	0.14	0.60	99.16	0.29	0.55	99.56	0.22	0.22
4	38.33	99.45	0.13	0.42	99.34	0.16	0.50	99.34	0.13	0.53	99.22	0.28	0.50	99.57	0.22	0.20
5	35.00	99.54	0.12	0.35	99.42	0.14	0.44	99.47	0.13	0.41	99.29	0.28	0.43	99.59	0.22	0.19
6	31.67	99.61	0.11	0.29	99.49	0.13	0.37	99.56	0.12	0.32	99.37	0.27	0.37	99.61	0.23	0.16
7	28.33	99.64	0.10	0.26	99.53	0.13	0.34	99.59	0.12	0.29	99.39	0.25	0.36	99.62	0.23	0.15
8	25.00	99.65	0.09	0.26	99.56	0.11	0.32	99.61	0.11	0.28	99.41	0.24	0.35	99.62	0.23	0.15
9	21.67	99.66	0.09	0.25	99.59	0.11	0.30	99.63	0.11	0.26	99.41	0.24	0.35	99.62	0.23	0.15
10	18.33	99.67	0.09	0.24	99.61	0.10	0.28	99.65	0.11	0.24	99.41	0.24	0.35	99.62	0.23	0.15
11	15.00	99.68	0.09	0.23	99.63	0.10	0.27	99.67	0.11	0.22	99.43	0.24	0.33	99.62	0.24	0.15
12	11.67	99.69	0.09	0.22	99.64	0.10	0.25	99.68	0.11	0.21	99.43	0.24	0.33	99.61	0.24	0.15
13	8.33	99.70	0.09	0.21	99.65	0.11	0.25	99.68	0.11	0.21	99.42	0.24	0.33	99.61	0.24	0.15
14	5.00	99.69	0.10	0.21	99.65	0.11	0.24	99.67	0.11	0.21	99.42	0.25	0.33	99.60	0.25	0.15
15	1.67	99.68	0.10	0.22	99.63	0.12	0.25	99.67	0.12	0.21	99.43	0.26	0.32	99.59	0.26	0.15
16	-1.67	99.68	0.10	0.22	99.63	0.12	0.25	99.67	0.12	0.21	99.43	0.26	0.31	99.59	0.26	0.15
17	-5.00	99.69	0.10	0.21	99.62	0.12	0.26	99.67	0.12	0.21	99.42	0.26	0.32	99.59	0.26	0.15
18	-8.33	99.68	0.11	0.22	99.62	0.12	0.26	99.67	0.12	0.20	99.42	0.26	0.32	99.59	0.26	0.15
19	-11.67	99.66	0.11	0.23	99.62	0.13	0.25	99.66	0.13	0.21	99.42	0.27	0.32	99.59	0.26	0.15
20	-15.00	99.65	0.11	0.25	99.61	0.13	0.26	99.66	0.13	0.21	99.41	0.27	0.32	99.59	0.26	0.15
21	-18.33	99.62	0.11	0.26	99.59	0.14	0.27	99.65	0.14	0.22	99.38	0.29	0.33	99.59	0.26	0.16
22	-21.67	99.60	0.12	0.28	99.58	0.14	0.28	99.62	0.15	0.23	99.36	0.30	0.34	99.58	0.26	0.16
23	-25.00	99.58	0.14	0.28	99.55	0.15	0.30	99.61	0.15	0.24	99.34	0.31	0.35	99.57	0.26	0.16
24	-28.33	99.56	0.16	0.29	99.52	0.17	0.31	99.58	0.16	0.26	99.30	0.32	0.38	99.57	0.26	0.17
25	-31.67	99.53	0.17	0.31	99.47	0.19	0.34	99.55	0.16	0.28	99.24	0.34	0.42	99.56	0.26	0.18
26	-35.00	99.45	0.18	0.37	99.41	0.20	0.39	99.47	0.17	0.36	99.15	0.35	0.50	99.54	0.27	0.19
27	-38.33	99.35	0.19	0.46	99.34	0.22	0.44	99.36	0.18	0.46	99.06	0.36	0.58	99.52	0.27	0.22
28	-41.67	99.27	0.21	0.52	99.30	0.23	0.47	99.27	0.19	0.55	98.97	0.37	0.66	99.50	0.27	0.23
29	-45.00	99.20	0.23	0.57	99.24	0.25	0.51	99.17	0.19	0.64	98.89	0.39	0.72	99.48	0.27	0.25
30	-48.33	99.11	0.25	0.65	99.17	0.26	0.56	99.08	0.21	0.71	98.80	0.40	0.80	99.44	0.27	0.28
CC4	-76.67	0.54	0.72	98.74	0.63	0.66	98.71	0.65	0.72	98.63	0.63	0.94	98.42	0.26	0.41	99.33
CC3	-80.00	0.45	0.84	98.71	0.56	0.74	98.70	0.56	0.86	98.58	0.56	1.06	98.38	0.24	0.46	99.30
CC2	-81.67	0.41	0.92	98.66	0.53	0.79	98.68	0.52	0.93	98.54	0.53	1.12	98.35	0.23	0.48	99.29
CC1	-83.33	0.38	1.01	98.61	0.48	0.85	98.67	0.48	1.03	98.49	0.50	1.19	98.31	0.22	0.50	99.28

Table 3. NOAA-L AMSU-A: The η factor in Equation (12).

Channel	f_{Asat} *(%)*	f_{sat} *(%)*	$\eta = f_{Asat}/f_{sat}$
1	*0.02*	*1.34*	*0.02*
2	*0.06*	*0.78*	*0.08*
3	*0.04*	*1.33*	*0.03*
4	*0.04*	*1.00*	*0.04*
5	*0.05*	*1.16*	*0.04*
6	*0.03*	*1.01*	*0.03*
7	*0.04*	*0.85*	*0.05*
8	*0.06*	*1.03*	*0.06*
9 - 14	*0.03*	*1.19*	*0.03*
15	*0.05*	*0.50*	*0.10*

4.4 Antenna Pattern Corrections

The calculated antenna efficiencies in Table 2 make it easy to perform any antenna pattern sidelobe correction. It has been shown that differences do occur between the true brightness temperatures and antenna temperatures observed by space-borne radiometers [3]-[7]. There are two main corrections which can be made with the efficiencies in Table 2. The first one is that the measurements at Earth views are contaminated by radiation which originates from the cold space and satellite platform. Similarly, measurements at the cold space views are contaminated by radiation from the Earth limbs and satellite platform. Table 2 shows that the antenna efficiencies over cold space are in the order of 1% at the edge of Earth views. In viewing the Earth scenes, this will reduce the observed antenna temperature by about the same percentages below the true brightness temperatures since the microwave cosmic background temperature $\overline{T}_C = 2.73$K is much smaller than the Earth's brightness temperature $\overline{T}_E$. In viewing cold space, the contamination introduced by the Earth limb can be 0.2% to 0.9% as shown in Table 2. This will produce an effective cold space calibration temperature higher than the nominal value of $\overline{T}_C = 2.73$K.

As discussed in Section 2, the quantity $\overline{T}_{Sat}$, which represents the total energy emanation associated with the satellite platform, may consist of satellite-platform radiation as well as reflected radiation from the Earth and cold space. The near-field radiation falls onto the antenna reflectors from all directions but only those parallel to the reflector axis are reflected to the feed horn at the focal point and detected. In practice, it is difficult (if it is not impossible) to select a single $\overline{T}_{Sat}$ value for representing these radiation sources. However, it has been shown elsewhere [3] that the maximum contribution due to this $\overline{T}_{Sat}$ in Equation (12) is only of the order of 0.01K. Therefore, the contribution from the last term in Equation (12) is negligibly small, particularly, in comparison to other uncertainties as discussed in [3]. Nevertheless, we retain this term with the knowledge that its effect on the final results is negligible.

To demonstrate the effect of the antenna pattern side lobes on the antenna temperatures, we apply Equation (12) to calculate a set of antenna temperatures, T_A, at the Earth scenes, using the calculated antenna efficiencies (Table 2), η values (Table 3), and a set of atmospheric brightness temperature profiles which correspond to an approximate estimate of AMSU-A measurements. Then, the antenna pattern corrections (of the Earth views), which are defined as $\Delta T = T_B - T_A$, are calculated. These calculated ΔT results are shown in Figure 3, which shows that Channel 1 has the largest ΔT and that the smallest ΔT occurs at Channel 15. Similarly, the antenna pattern corrections at the space views, $\Delta T_C = T_A - 2.73K$, were also calculated and the results are shown in Table 4, which shows the cold calibration position 1 (CC1) has the least contamination.

The $\overline{T_E}$ values used in this simulation are 230K for Channels 1-4 and 15, 240K for Channel 5, and 210K for Channels 6-9, respectively. For the four cold space calibration positions, $\overline{T_E} = 210K$ were used to calculate the antenna temperatures (see discussion in Section 2). The ΔT values in Figure 3 correspond to fixed biases in the antenna system and should be added to the antenna temperatures to obtain the true brightness temperatures. Similarly, the ΔT_C values in Table 4 should be combined with T_C (=2.73K) to obtain a set of "effective" cold space calibration temperatures, which are required in the NESDIS operational Calibration Parameters Input Data Set (CPIDS) for generating the calibration coefficients. After launch, the in-orbit data will be analyzed to verify these predicted values.

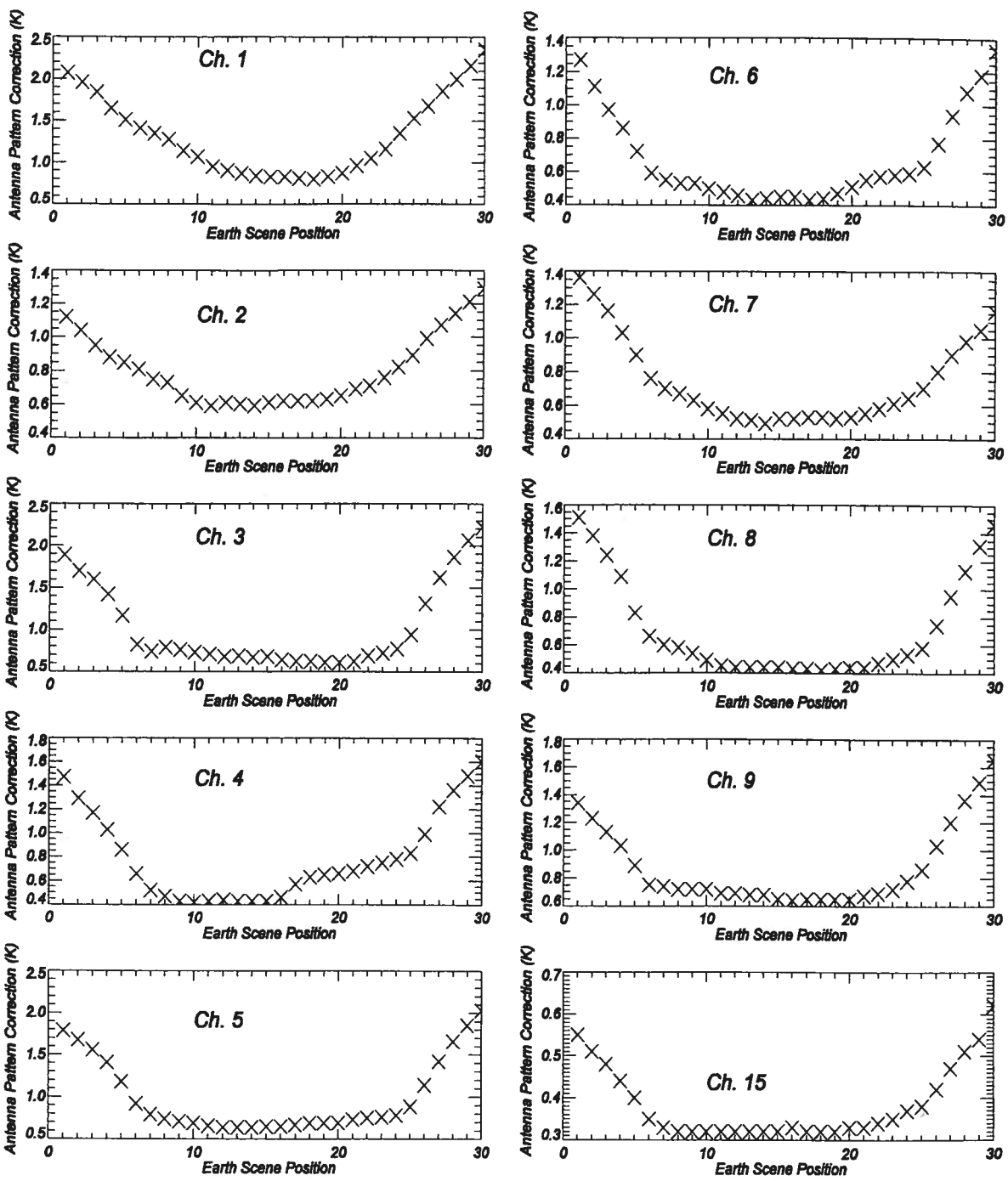

Figure 3. Sample of calculated NOAA-L antenna pattern corrections $\Delta T = T_B - T_A$ for one scan line.

Table 4. NOAA-L: Cold space bias correction, ΔT_C(K), to the cosmic background temperature ($T_C = 2.73 + \Delta Tc$). These values were calculated using AMSU-A1 PFM and A2 FM1 antenna pattern data

Position	Angle	Ch.1	2	3	4	5	6	7	8	9-14	15
CC4	-76.67	1.97	1.00	2.10	1.31	1.61	1.26	1.47	1.56	1.48	0.80
CC3	-80.00	1.77	0.89	1.92	1.18	1.48	1.07	1.32	1.40	1.34	0.77
CC2	-81.67	1.65	0.84	1.84	1.13	1.42	1.00	1.25	1.33	1.28	0.75
CC1	-83.33	1.55	0.80	1.75	1.06	1.35	0.94	1.17	1.26	1.22	0.74

5. Conclusion

This study provides detailed information about the measured antenna pattern data from the NOAA-L and -M AMSU-A instruments and presents a procedure for performing antenna pattern sidelobe corrections to antenna temperatures. The 3-dB beamwidths and main beam efficiencies were also calculated from the antenna pattern data for comparison with the AMSU-A specifications of 95% (or better) for the main beam efficiencies and $3.3^{\circ} \pm 10\%$ for the 3-dB beamwidths.

Predictions of antenna pattern sidelobe corrections were made over three solid-angle regions subtended at the satellite by the Earth (plus 20-km atmosphere), cold space, and the satellite platform. Antenna efficiencies over these three solid-angle regions were calculated at 30 Earth views and 4 possible cold space calibration views (one of which will be selected after launch) of the AMSU-A scan operation. These calculated antenna efficiencies make it possible to perform antenna pattern sidelobe corrections. A simulation using these antenna efficiencies and a profile of atmospheric brightness temperatures shows that the resultant antenna sidelobe corrections can be more than 2K (Figure 3) for some channel fields of view on the edges of scan swatch where more cold space radiance is sensed via the antenna side lobes.

Contribution from the satellite platform (the last term in Equation 12) is negligibly small with a magnitude less than 0.01K, which is much less than other measurement uncertainties [3].

Computations of the antenna pattern corrections at the four possible cold space calibration positions reveal that the space view CC1 for all channels has the least contamination from the Earth and satellite

platform. One should note that an optimal choice of the cold space views will be made after each launch of AMSU-A and that these antenna pattern corrections will be compared to those obtained using the in-orbit data during the instrument's activation and evaluation period.

The antenna efficiencies presented in this study make it easy to design an algorithm for performing antenna pattern corrections to the antenna temperatures from the AMSU-A data. These antenna efficiencies will be made available to AMSU-A data users who want to make appropriate corrections for improving the accuracy of the data.

ACKNOWLEDGMENT: Aerojet is the primary contractor for building the AMSU-A instruments and measured the antenna patterns used in this study.

REFERENCES

[1]. T. Mo, "Prelaunch Calibration of the Advanced Microwave Sounding Unit-A for NOAA-K," IEEE Trans. Microwave Theory and Techniques, vol. 44, pp. 1460-1469, 1996.

[2]. R. W. Rogers, T. J. Hewison, N. C. Atkinson, and S. J. Stringer, "The radiometric Characterization of AMSU-B," IEEE Trans. Microwave Theory and Techniques, vol. 43, pp. 760-771, 1995.

[3]. Tsan Mo, "AMSU-A Antenna Pattern Corrections," IEEE Trans. Geoscience and Remote Sensing, vol. 37, pp. 103-112, January 1999.

[4]. J. P. Classen and A. K. Fung, "The Recovery of Polarized Apparent Temperature Distributions of Flat Scenes from Antenna Temperature Measurements," IEEE Trans. Antennas and Propagation, vol. AP-22, pp. 433-442, May 1974.

[5]. E. G. Njoku, "Antenna Pattern Correction Procedures for the Scanning Multichannel Microwave Radiometer (SMMR), "Boundary-Layer Meteorology, vol. 18, pp. 79-98, 1980.

[6]. T. J. Hewsion and R. Saunders, "Measurements of the AMSU-B Antenna Pattern," IEEE Trans. Geoscience and Remote Sensing, vol. 34, pp. 405-412, March 1996.

[7]. D. Brest, GenCorp Aerojet, Azusa, CA, 1997, private communication.

[8] "Calibration Log Book for AMSU-A2 S/N 103," Report No. 10480A, September 1995, Aerojet, Azusa, CA 91702.

[9] "Calibration Log Book for AMSU-A1 S/N 102," Report No. 10643AA, September 1995, Aerojet, Azusa, CA 91702.

[10] "Calibration Log Book for AMSU-A2 S/N 104," Report No. 10637A, September 1995, Aerojet, Azusa, CA 91702.

[11] "Calibration Log Book for AMSU-A1 S/N 104," Report No. 1064A, September 1995, Aerojet, Azusa, CA 91702.

[12] "AMSU-A Verification Test Report," Report No. 9875-3A, June 1994, Aerojet, Azusa, CA 91702.

APPENDIX A

NOAA-M AMSU-A ANTENNA PATTERN CORRECTIONS

The NOAA-M AMSU-A antenna pattern corrections calculated from the measured antenna pattern data are presented here in a similar fashion as those for NOAA-L AMSU-A results given in the main text. Tables and plots of results follow the same order as the NOAA-L cases as closely as possible.

Table A-1 lists the NOAA-M AMSU-A1 and AMSU-A2 FM2 channel characteristics. The calculated NOAA-M AMSU-A antenna efficiencies are given in Table A-2. The η factors for NOAA-M AMSU-A and the cold space bias corrections are presented in Tables A-3 and A-4, respectively.

Figure A-1 shows a sample of antenna pattern data from AMSU-A1 FM2 Channel 3 (50.3 GHz). A sample of calculated NOAA-M antenna pattern corrections for one scan line is shown in Figure A-2.

Table A-1. NOAA-M AMSU-A1 FM2 and AMSU-A2 FM2 channel characteristics.

Channel Number	Channel Frequency (MHz)		No. of Bands	Measured 3-dB RF Bandwidth (MHz)	NEΔT (K)		Beam # Effici.	Polarization (NADIR)	FOV** (deg.)	Remarks
	Specification	Measured *			Spec	Measred				
1	23800	23799.21	1	251.02	0.30	0.152	97%	V	3.60	A2 FM2
2	31400	31399.66	1	161.16	0.30	0.209	99%	V	3.51	"
3	50300	50299.18	1	161.16	0.40	0.297	96%	V	3.57	A1-2 FM2
4	52800	52800.80	1	380.42	0.25	0.155	95%	V	3.45	"
5	53596 ± 115	53596.60 ± 115	2	168.15 I 168.15	0.25	0.148	95%	H	3.53	"
6	54400	54400.24	1	380.52	0.25	0.154	96%	H	3.41	A1-1 FM2
7	54940	54939.82	1	380.60	0.25	0.167	96%	V	3.42	"
8	55500	55499.20	1	310.20	0.25	0.150	96%	H	3.45	A1-2 FM2
9	fo = 57290.344	fo = 57290.343	1	309.82	0.25	0.170	96%	H	3.37	A1-1 FM2
10	fo ± 217	fo ± 217	2	76.65 I 76.65	0.40	0.208		H		"
11	fo ± 322.2 ± 48	fo ± 322.2 ± 48	4	34.86 / 34.67 I 34.67 / 34.86	0.40	0.254		H		"
12	fo ± 322.2 ± 22	fo ± 322.2 ± 22	4	15.07 / 15.29 I 15.29 / 15.07	0.60	0.349		H		"
13	fo ± 322.2 ± 10	fo ± 322.2 ± 10	4	7.88 / 7.92 I 7.92 / 7.88	0.80	0.482		H		"
14	fo ± 322.2 ± 4.5	fo ± 322.2 ± 4.5	4	2.87 / 2.94 I 2.94 / 2.87	1.20	0.830		H		"
15	89000	89000.10	1	1998.86	0.50	0.147	96%	V	3.17	"

, # Measured at temperature 18°C. ** Specification= 3.3° ±10% for all channels. # Measured

Table A-2. NOAA-M AMSU-A antenna efficiencies over Earth, spacecraft, and cold space.

Beam Pos.	Scan Angle (deg.)	Ch.1			Ch.2			Ch.3			Ch.4			Ch.5		
		Fearth (%)	Fsat (%)	Fspace (%)	Fearth (%)	Fsat (%)	Fspace (%)	Fearth (%)	Fsat (%)	Fspace (%)	Fearth (%)	Fsat (%)	Fspace (%)	Fearth (%)	Fsat (%)	Fspace (%)
1	48.33	98.78	0.31	0.91	99.38	0.13	0.49	98.88	0.29	0.83	99.22	0.13	0.65	99.05	0.19	0.76
2	45.00	98.87	0.27	0.86	99.43	0.11	0.46	98.98	0.27	0.75	99.31	0.12	0.57	99.13	0.16	0.71
3	41.67	98.96	0.23	0.81	99.48	0.10	0.42	99.05	0.24	0.71	99.37	0.12	0.52	99.20	0.14	0.66
4	38.33	99.07	0.21	0.73	99.52	0.09	0.39	99.14	0.23	0.63	99.44	0.11	0.45	99.28	0.13	0.59
5	35.00	99.15	0.18	0.67	99.55	0.08	0.38	99.28	0.21	0.52	99.52	0.10	0.38	99.38	0.12	0.50
6	31.67	99.22	0.16	0.62	99.57	0.07	0.36	99.43	0.20	0.36	99.61	0.10	0.29	99.50	0.11	0.39
7	28.33	99.26	0.15	0.59	99.60	0.07	0.33	99.49	0.18	0.33	99.68	0.09	0.23	99.56	0.11	0.34
8	25.00	99.31	0.13	0.56	99.61	0.06	0.32	99.50	0.15	0.35	99.70	0.09	0.21	99.58	0.11	0.31
9	21.67	99.38	0.12	0.50	99.65	0.06	0.29	99.53	0.14	0.33	99.72	0.09	0.19	99.59	0.10	0.30
10	18.33	99.42	0.11	0.47	99.67	0.06	0.27	99.54	0.14	0.32	99.72	0.09	0.19	99.61	0.10	0.29
11	15.00	99.47	0.11	0.42	99.68	0.06	0.26	99.56	0.13	0.31	99.71	0.09	0.19	99.63	0.09	0.28
12	11.67	99.49	0.11	0.40	99.68	0.06	0.27	99.57	0.13	0.30	99.71	0.10	0.19	99.64	0.09	0.27
13	8.33	99.51	0.11	0.38	99.68	0.06	0.26	99.56	0.13	0.31	99.71	0.10	0.19	99.64	0.09	0.27
14	5.00	99.52	0.11	0.37	99.68	0.06	0.26	99.57	0.13	0.30	99.71	0.10	0.19	99.63	0.09	0.27
15	1.67	99.52	0.11	0.37	99.66	0.07	0.27	99.57	0.13	0.30	99.71	0.10	0.19	99.63	0.10	0.28
16	-1.67	99.53	0.11	0.36	99.66	0.07	0.28	99.58	0.14	0.28	99.69	0.11	0.21	99.63	0.10	0.28
17	-5.00	99.54	0.11	0.36	99.66	0.07	0.27	99.59	0.14	0.27	99.64	0.11	0.25	99.62	0.10	0.28
18	-8.33	99.54	0.11	0.35	99.65	0.07	0.28	99.59	0.14	0.27	99.62	0.11	0.28	99.61	0.10	0.29
19	-11.67	99.52	0.11	0.37	99.65	0.07	0.28	99.59	0.14	0.27	99.60	0.11	0.29	99.61	0.10	0.29
20	-15.00	99.50	0.11	0.38	99.63	0.08	0.29	99.59	0.15	0.27	99.59	0.12	0.29	99.60	0.11	0.29
21	-18.33	99.45	0.12	0.42	99.61	0.09	0.30	99.57	0.16	0.28	99.57	0.13	0.30	99.58	0.12	0.31
22	-21.67	99.41	0.13	0.46	99.59	0.09	0.31	99.52	0.17	0.30	99.54	0.14	0.32	99.56	0.13	0.32
23	-25.00	99.35	0.14	0.51	99.57	0.10	0.33	99.50	0.18	0.32	99.52	0.15	0.33	99.54	0.14	0.32
24	-28.33	99.26	0.15	0.59	99.53	0.11	0.36	99.47	0.19	0.34	99.50	0.16	0.35	99.52	0.15	0.33
25	-31.67	99.17	0.16	0.67	99.49	0.12	0.40	99.37	0.22	0.41	99.45	0.18	0.37	99.47	0.16	0.37
26	-35.00	99.09	0.17	0.74	99.43	0.13	0.44	99.19	0.23	0.58	99.35	0.21	0.44	99.34	0.18	0.48
27	-38.33	98.99	0.19	0.82	99.39	0.14	0.47	99.05	0.24	0.71	99.23	0.23	0.54	99.21	0.19	0.60
28	-41.67	98.91	0.21	0.88	99.34	0.16	0.51	98.92	0.26	0.82	99.15	0.25	0.60	99.10	0.20	0.70
29	-45.00	98.80	0.25	0.95	99.28	0.18	0.53	98.82	0.27	0.91	99.07	0.27	0.65	99.00	0.22	0.78
30	-48.33	98.68	0.29	1.03	99.23	0.21	0.57	98.71	0.31	0.98	99.00	0.30	0.71	98.90	0.24	0.86
CC4	-76.67	0.90	1.07	98.02	0.40	0.63	98.97	0.90	1.10	98.00	0.55	0.83	98.62	0.67	0.88	98.45
CC3	-80.00	0.80	1.19	98.00	0.34	0.70	98.96	0.82	1.21	97.97	0.49	0.91	98.60	0.60	1.01	98.39
CC2	-81.67	0.75	1.26	98.00	0.31	0.74	98.95	0.77	1.27	97.96	0.46	0.95	98.59	0.57	1.08	98.35
CC1	-83.33	0.69	1.34	97.97	0.29	0.78	98.93	0.73	1.33	97.95	0.43	1.00	98.57	0.53	1.16	98.30

Beam Pos.	Scan Angle (deg.)	Ch. 6			Ch. 7			Ch. 8			Ch. 9			Ch. 15		
		Fearth (%)	Fsat (%)	Fspace (%)	Fearth (%)	Fsat (%)	Fspace (%)	Fearth (%)	Fsat (%)	Fspace (%)	Fearth (%)	Fsat (%)	Fspace (%)	Fearth (%)	Fsat (%)	Fspace (%)
1	48.33	99.22	0.17	0.61	99.14	0.20	0.66	99.09	0.18	0.73	99.03	0.32	0.65	99.53	0.22	0.25
2	45.00	99.30	0.16	0.54	99.21	0.18	0.61	99.17	0.16	0.67	99.09	0.31	0.60	99.54	0.22	0.23
3	41.67	99.38	0.15	0.47	99.27	0.17	0.56	99.26	0.14	0.60	99.16	0.29	0.55	99.56	0.22	0.22
4	38.33	99.45	0.13	0.42	99.34	0.16	0.50	99.34	0.13	0.53	99.22	0.28	0.50	99.57	0.22	0.20
5	35.00	99.54	0.12	0.35	99.42	0.14	0.44	99.47	0.13	0.41	99.29	0.28	0.43	99.59	0.22	0.19
6	31.67	99.61	0.11	0.29	99.49	0.13	0.37	99.56	0.12	0.32	99.37	0.27	0.37	99.61	0.23	0.16
7	28.33	99.64	0.10	0.26	99.53	0.13	0.34	99.59	0.12	0.29	99.39	0.25	0.36	99.62	0.23	0.15
8	25.00	99.65	0.09	0.26	99.56	0.11	0.32	99.61	0.11	0.28	99.41	0.24	0.35	99.62	0.23	0.15
9	21.67	99.66	0.09	0.25	99.59	0.11	0.30	99.63	0.11	0.26	99.41	0.24	0.35	99.62	0.23	0.15
10	18.33	99.67	0.09	0.24	99.61	0.10	0.28	99.65	0.11	0.24	99.41	0.24	0.35	99.62	0.23	0.15
11	15.00	99.68	0.09	0.23	99.63	0.10	0.27	99.67	0.11	0.22	99.43	0.24	0.33	99.62	0.24	0.15
12	11.67	99.69	0.09	0.22	99.64	0.10	0.25	99.68	0.11	0.21	99.43	0.24	0.33	99.61	0.24	0.15
13	8.33	99.70	0.09	0.21	99.65	0.11	0.25	99.68	0.11	0.21	99.42	0.24	0.33	99.61	0.24	0.15
14	5.00	99.69	0.10	0.21	99.65	0.11	0.24	99.67	0.11	0.21	99.42	0.25	0.33	99.60	0.25	0.15
15	1.67	99.68	0.10	0.22	99.63	0.12	0.25	99.67	0.12	0.21	99.43	0.26	0.32	99.59	0.26	0.15
16	-1.67	99.68	0.10	0.22	99.63	0.12	0.25	99.67	0.12	0.21	99.43	0.26	0.31	99.59	0.26	0.15
17	-5.00	99.69	0.10	0.21	99.62	0.12	0.26	99.67	0.12	0.21	99.42	0.26	0.32	99.59	0.26	0.15
18	-8.33	99.68	0.11	0.22	99.62	0.12	0.26	99.67	0.12	0.20	99.42	0.26	0.32	99.59	0.26	0.15
19	-11.67	99.66	0.11	0.23	99.62	0.13	0.25	99.66	0.13	0.21	99.42	0.27	0.32	99.59	0.26	0.15
20	-15.00	99.65	0.11	0.25	99.61	0.13	0.26	99.66	0.13	0.21	99.41	0.27	0.32	99.59	0.26	0.15
21	-18.33	99.62	0.11	0.26	99.59	0.14	0.27	99.65	0.14	0.22	99.38	0.29	0.33	99.59	0.26	0.16
22	-21.67	99.60	0.12	0.28	99.58	0.14	0.28	99.62	0.15	0.23	99.36	0.30	0.34	99.58	0.26	0.16
23	-25.00	99.58	0.14	0.28	99.55	0.15	0.30	99.61	0.15	0.24	99.34	0.31	0.35	99.57	0.26	0.16
24	-28.33	99.56	0.16	0.29	99.52	0.17	0.31	99.58	0.16	0.26	99.30	0.32	0.38	99.57	0.26	0.17
25	-31.67	99.53	0.17	0.31	99.47	0.19	0.34	99.55	0.16	0.28	99.24	0.34	0.42	99.56	0.26	0.18
26	-35.00	99.45	0.18	0.37	99.41	0.20	0.39	99.47	0.17	0.36	99.15	0.35	0.50	99.54	0.27	0.19
27	-38.33	99.35	0.19	0.46	99.34	0.22	0.44	99.36	0.18	0.46	99.06	0.36	0.58	99.52	0.27	0.22
28	-41.67	99.27	0.21	0.52	99.30	0.23	0.47	99.27	0.19	0.55	98.97	0.37	0.66	99.50	0.27	0.23
29	-45.00	99.20	0.23	0.57	99.24	0.25	0.51	99.17	0.19	0.64	98.89	0.39	0.72	99.48	0.27	0.25
30	-48.33	99.11	0.25	0.65	99.17	0.26	0.56	99.08	0.21	0.71	98.80	0.40	0.80	99.44	0.27	0.28
CC4	-76.67	0.54	0.72	98.74	0.63	0.66	98.71	0.65	0.72	98.63	0.63	0.94	98.42	0.26	0.41	99.33
CC3	-80.00	0.45	0.84	98.71	0.56	0.74	98.70	0.56	0.86	98.58	0.56	1.06	98.38	0.24	0.46	99.30
CC2	-81.67	0.41	0.92	98.66	0.53	0.79	98.68	0.52	0.93	98.54	0.53	1.12	98.35	0.23	0.48	99.29
CC1	-83.33	0.38	1.01	98.61	0.48	0.85	98.67	0.48	1.03	98.49	0.50	1.19	98.31	0.22	0.50	99.28

Table A-3. NOAA-M AMSU-A: The η factor in Eq. (12).

Channel	f_{Asat} (%)	f_{sat} (%)	$\eta = f_{Asat}/f_{sat}$
1	0.02	0.78	0.03
2	0.06	0.57	0.11
3	0.04	1.23	0.03
4	0.04	1.46	0.03
5	0.05	1.45	0.03
6	0.03	1.06	0.03
7	0.04	1.24	0.03
8	0.06	1.24	0.05
9 - 14	0.03	0.88	0.03
15	0.05	0.75	0.07

Table A-4. NOAA-M: Cold space bias correction, ΔTc(K), to the cosmic background temperature (Tc= 2.73 + ΔTc). These values were calculated using AMSU-A1 FM2 and A2 FM2 antenna pattern data

Position	Angle	Ch.1	2	3	4	5	6	7	8	9-14	15
CC4	-76.67	0.93	0.60	1.41	2.27	2.02	1.46	1.64	1.84	1.40	0.82
CC3	-80.00	0.82	0.51	1.26	2.02	1.78	1.27	1.47	1.65	1.27	0.76
CC2	-81.67	0.79	0.49	1.20	1.91	1.66	1.22	1.37	1.55	1.21	0.73
CC1	-83.33	0.76	0.48	1.12	1.79	1.54	1.16	1.28	1.45	1.16	0.71

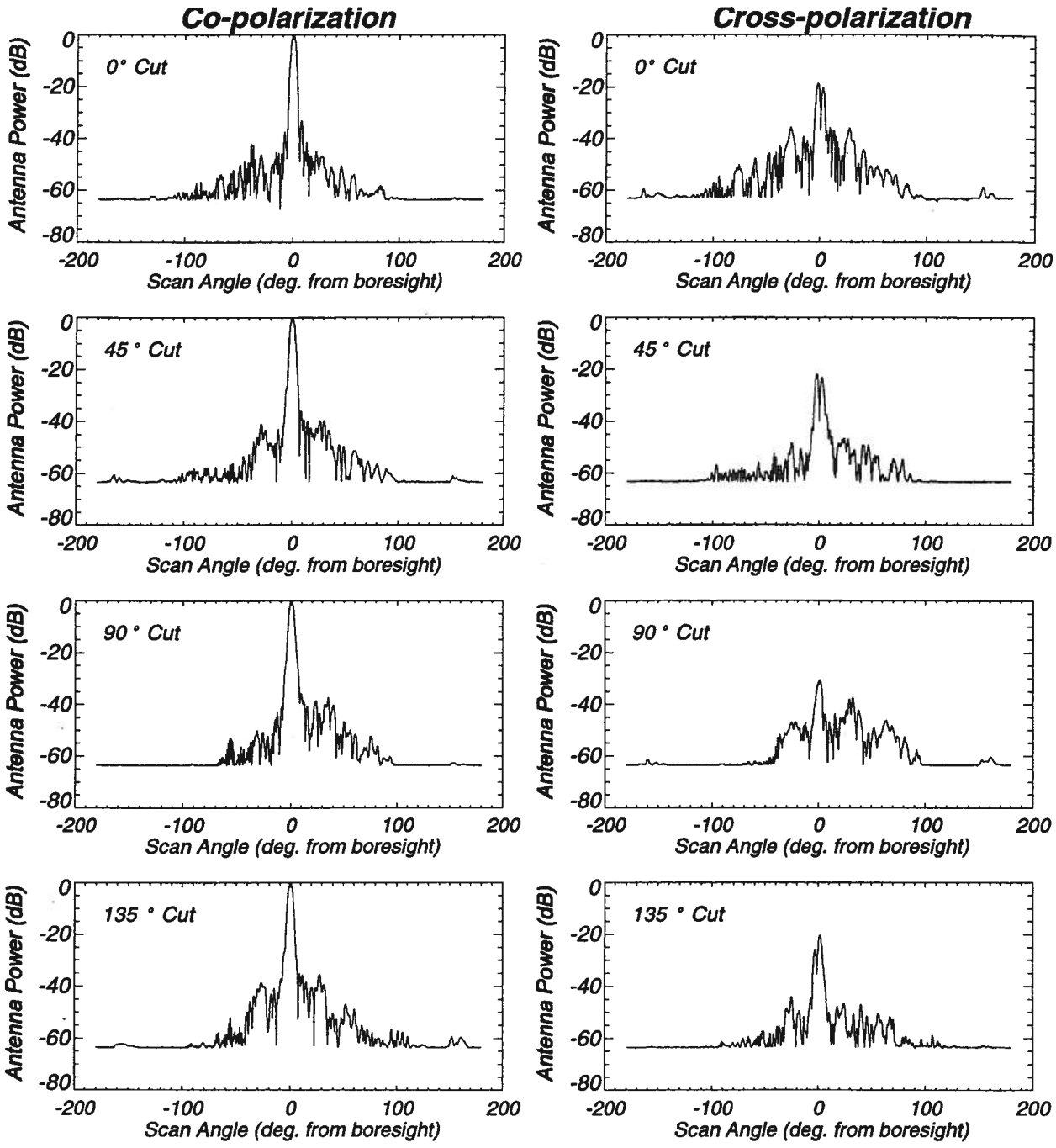

Figure A-1. Sample of antenna pattern data from AMSU-A1 FM2 Channel 3 (50.3 GHz). The left-hand column shows the co-polarized data whereas the cross-polarized data are displayed in the right-hand column.

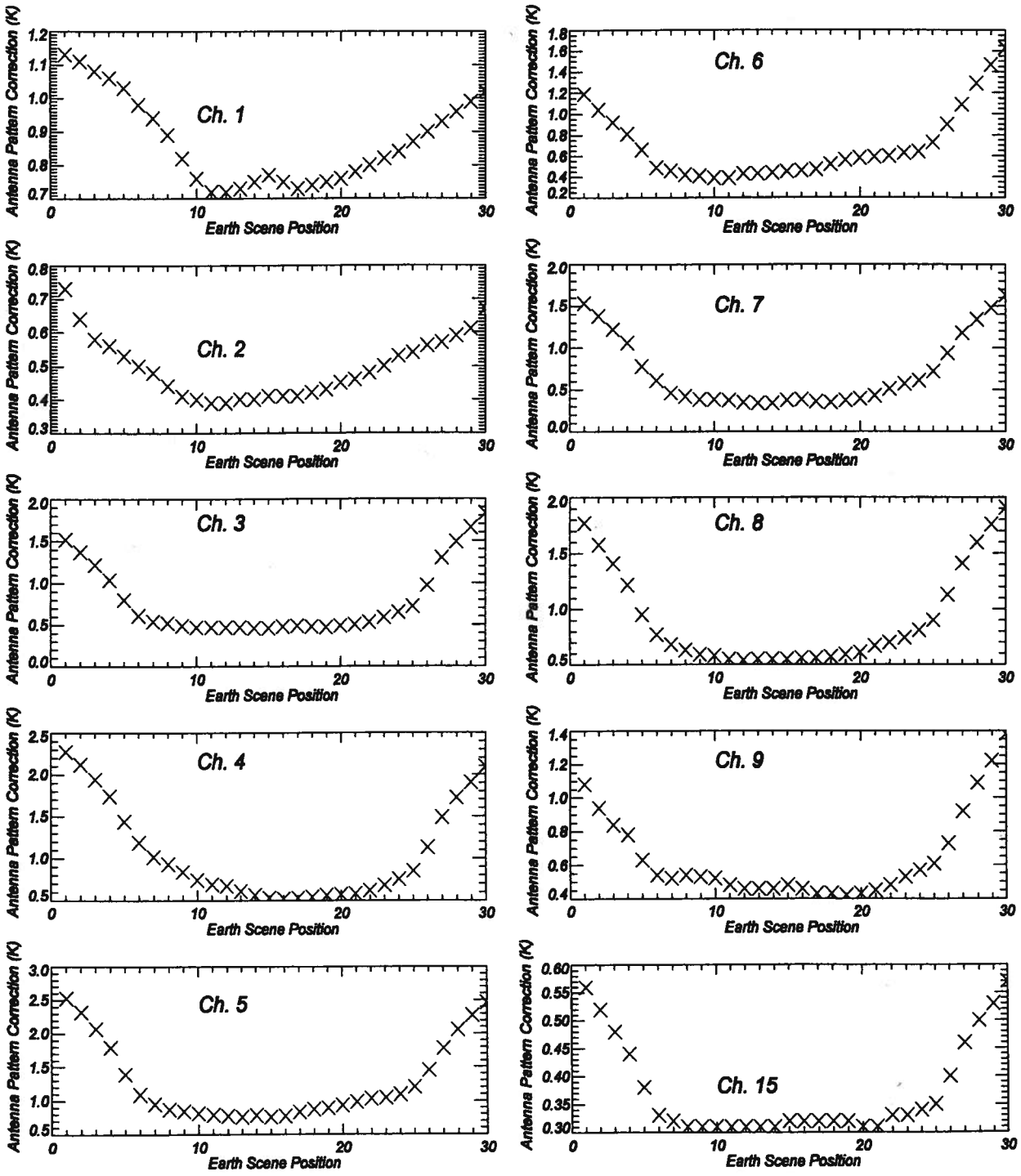

Figure A-2. Sample of calculated NOAA-M antenna pattern corrections $\Delta T = T_B - T_A$ for one scan line.

NESDIS 69 Nonlinearity Corrections for the Thermal Infrared Channels of the Advanced Very High Resolution Radiometer: Assessment and Recommendations. C.R. N. Rao (Editor), June 1993.

NESDIS 70 Degradation of the Visible and Near-Infrared Channels of the Advanced Very High Resolution Radiometer on the NOAA-9 Spacecraft: Assessment and Recommendations for Corrections. C.R. N. Rao (Editor), June 1993.

NESDIS 71 Spectral Radiance-Temperature Conversions for Measurements by AVHRR Thermal Channels 3,4,5. Paul A. Davis, August 1993.

NESDIS 72 Summary of the NOAA/NESDIS Workshop on Development of a Global Satellite/in Situ Environmental Database. Edited by K.P. Gallo and D.A. Hastings, August 1993.

NESDIS 73 Intercomparison of the Operational Calibration of GOES-7 and METEOSAT-3/4. W. Paul Menzel, Johannes Schmetz, Steve Nieman, Leo Van de Berg, Volker Gaertner, and Timothy J. Schmit, September 1993.

NESDIS 74 Dobson Data Re-Evaluation Handbook. R. D. Hudson and W.G. Planet (Eds), October 1993.

NESDIS 75 Detection and Analysis of Fog at Night Using GOES Multispectral. Gary P. Ellrod, February 1994.

NESDIS 76 Tovs Operational Sounding Upgrades: 1990-1992. A. Reale, M. Chalfant, R. Wagoner, T. Gardner and L. Casey, March 1994.

NESDIS 77 NOAA Polar Satellite Calibration: A System Description. Cecil A. Paris, April 1994.

NESDIS 78 Post-Launch Calibration of the Visible and Near Infrared Channels of the Advanced Very High Resolution Radiometer on NOAA-7,-9, and -11 Spacecraft. C. R. Nagaraja Rao and Jianhua Chen, April 1994.

NESDIS 79 Quality Control and Processing of Historical Oceanographic Nutrient Data. Margarita E. Conkright, Timothy P. Boyer and Sydney Levitus, April 1994.

NESDIS 80 Catalogue of Heavy Rainfall Cases of Six Inches or More Over the Continental U.S. During 1993. Richard Borneman and Charles Kadin, August 1994.

NESDIS 81 Quality Control and Processing of Historical Oceanographic Temperature, Salinity, and Oxygen Data. Timothy Boyer and Sydney Levitus, August 1994.

NESDIS 82 An Introduction to the GOES I-M Imagr and Sounder Instruments and the GVAR Retransmission Format. Raymond Komajda (Mitre Corp), November 1994.

NESDIS 83 Tropical Cyclone Motion Forecasting Using Satellite Water Vapor Imagery. Vernon F. Dvorak and H. Michael Mogil, December 1994.

NESDIS 84 Spurious Semi-Diurnal Variation in the E.R.B.E. Outgoing Longwave Radiation. C. R. Kondragunta and Arnold Gruber, June 1995.

NESDIS 85 Calibration of the Advanced Microwave Sounding Unit-A for NOAA-K. Tsan Mo, June 1995.

NESDIS 86 A Spectral pproasch to the Forward Problem in GPS Radio Occulation Remote Sensing (Ray Tracing, Assimilation, Tomography). Simon Rosenfeld, July 1996.

NESDIS 87 Proceedings of the International Workshop on Oceanographic Biological and Chemical Data Management. Sponsors Intergovernmental Oceanographic Commission, U.S. National Oceanographic Data Center, European Union MAST Programme, May 1996.

NESDIS 88 Analytical Model of Refraction in a Moist Polytropic Atmosphere for Space and Ground-Based GPS Applications. Simon Rosenfeld, April 1997.

NESDIS 89 A GOES Image Quality Analysis System for the NOAA/NESDIS Satellite Operations Control Center. Donald H. Hillger and Peter J. Celone, December 1997.

NESDIS 90 Automated Satellite-Based Estimates of Precipitation: An Assessment of Accuracy. Michael A. Fortune, June 1998.

NESDIS 91 Aliasing of Satellite Altimeter Data in Exact-Repeat Sampling Mode: Analytic Formulas for the Mid-Point Grid. Chang-Kou Tai, March 1999.

NESDIS 92 Calibration of the Advanced Microwave Sounding Unit-A Radiometers for NOAA-L and NOAA-M. Tsan Mo, May 1999.

NESDIS 93 GOES Imager and Sounder Calibration, Scaling, and Image Quality. Donald W. Hillger, June 1999.

NESDIS 94 MSU Antenna Pattern Data. Tsan Mo, March 2000.

NOAA SCIENTIFIC AND TECHNICAL PUBLICATIONS

The National Oceanic and Atmospheric Administration **was established as part of the Department of Commerce on October 3, 1970. The mission responsibilities of NOAA are to assess the socioeconomic impact of natural and technological changes in the environment and to monitor and predict the state of the solid Earth, the oceans and their living resources, the atmosphere, and the space environment of the Earth.**

The major components of NOAA regularly produce various types of scientific and technical information in the following types of publications:

PROFESSIONAL PAPERS - Important definitive research results, major techniques, and special investigations.

CONTRACT AND GRANT REPORTS - Reports prepared by contractors or grantees under NOAA sponsorship.

ATLAS - Presentation of analyzed data generally in the form of maps showing distribution of rainfall, chemical and physical conditions of oceans and atmosphere, distribution of fishes and marine mammals, ionospheric conditions, etc.

TECHNICAL SERVICE PUBLICATIONS - Reports containing data, observations, instructions, etc. A partial listing includes data serials; prediction and outlook periodicals; technical manuals, training papers, planning reports, and information serials; and miscellaneous technical publications.

TECHNICAL REPORTS - Journal quality with extensive details, mathematical developments, or data listings.

TECHNICAL MEMORANDUMS - Reports of preliminary, partial, or negative research or technology results, interim instructions, and the like.

U.S. DEPARTMENT OF COMMERCE
National Oceanic and Atmospheric Administration
National Environmental Satellite, Data, and Information Service
Washington, D.C. 20233